

## Influence of Annealing treatment on Microstructure and Properties of Cold-drawn Al-3.0wt.%Mg Alloy

Xin Zhang\*, Ruiqi Ma, Zehua Wang, Zehua Zhou, Guangheng Yang, Xin Cai

College of Mechanics and Materials, Hohai University, Nanjing, 210098, China

\*E-mail: [zhangxin.007@163.com](mailto:zhangxin.007@163.com)

Received: 2 October 2020 / Accepted: 11 November 2020 / Published: 30 November 2020

---

The influence of annealing treatment on the microstructure, mechanical properties and corrosion behavior of cold-drawn Al-3.0 wt%Mg alloy was investigated by 2D-XRD, microstructure observation, tensile test, immersion test and electrochemical measurement. The relationships between microstructure and mechanical properties of the annealed alloy wire at different temperatures were studied. The result showed that during the annealing process, recrystallized grain appeared, and there was no reaction on the second phase particles. At the same time, the intensity of deformation texture decreased, while recrystallization texture appeared. With the increase in the annealing temperature, the tensile strength of the alloy decreased linearly, while the yield strength exhibited a three-stage characteristic decrease, and the elongation to failure first increased and then decreased. In addition, there was a linear relationship between the texture intensity, grain size and the strength of the alloy wire. The annealed alloy had a better corrosion resistance than the cold-drawn alloy. However, the annealed and cold-drawn alloys had similar pitting corrosion sensibility.

---

**Keywords:** Al-3.0 wt.%Mg alloy; cold-drawn wire; annealing temperature; mechanical properties; corrosion behaviour

### 1. INTRODUCTION

Al-Mg alloys have excellent comprehensive properties including high specific strength and ductility, low electric resistivity, and excellent corrosion resistance, and are considered as the novel electromagnetic shielding materials [1-3]. Al-Mg alloy electromagnetic shielding wires are usually prepared by cold-drawing processing. However, during the cold-drawing process, material hardening occurs significantly, and the plasticity decreases dramatically [4-10]. Excessive cold-drawing processing can cause a range of structural defects and reduce the plasticity and toughness of the alloys, which is harmful to the subsequent drawing and weaving processing. Therefore, heat treatment is needed to improve the microstructure and properties of cold-drawn alloy wires.

As mentioned above, as the cold-drawing strain increased, the strength of Al-3.0 wt.%Mg alloy increased linearly, while the plasticity exhibited a three-stage characteristic decrease. When the strain achieved 96%, the plasticity of the cold-drawn Al-3.0 wt.%Mg alloy decreased to 3.13% and it was hard to be processed continuously [11]. At the same time, as the strain increased, the corrosion resistance increased, the pitting sensibility decreased, and the corrosion sensibility first increased and then decreased [12]. As a result, heat treatment should be studied to improve the mechanical properties and corrosion resistance of Al-3.0 wt.% Mg alloy for the subsequent processing.

In this paper, the influence of annealing treatment on the microstructure, mechanical properties and corrosion behavior of the cold-drawn Al-3.0 wt.%Mg alloy wire with 96% strain was studied. The results clarified the relationship between the microstructure evolution and property change of the alloy wires during the annealing treatment, and prepared for the subsequent drawing and weaving processing.

## 2. EXPERIMENTAL

### 2.1 Material preparation

An electrical resistance furnace was used to prepare Al-3.0 wt.%Mg alloy from A00 aluminum ingot (99.7 wt.%) and magnesium ingot (99.9 wt.%) in a graphite crucible at 720 °C. After the aluminum ingot was completely melted at 720 °C, pure magnesium ingot was pressed into the molten aluminum, and held for 10 min to ensure that the added magnesium was completely dissolved. The sample was degassed with argon for 10 min before pouring into a metal mould at 720 °C. Finally, a dense test bar was obtained and processed into a rod with a diameter of  $\Phi 10$  mm. As shown in Table 1, the actual compositions of the alloy rod were obtained.

**Table 1.** The actual compositions of Al-3.0 wt.%Mg alloy

Element	Mg	Si	Fe	Al
wt.%	3.02	0.12	0.17	<i>Bal.</i>

### 2.2 Cold-drawing process and annealing treatment

Before the cold-drawing processing of the rod alloy, the homogenizing annealing was carried out at 445 °C for 5 hours. Then, the Al-3.0 wt.%Mg alloy wire was manufactured by a LWD650-1200 wire drawing machine. A low drawing speed of 10 m/min was applied in the drawing process. The total area reduction of the alloy wire was 96%, and 15 passes were adopted from the  $\Phi 10$  mm rod to the  $\Phi 2$  mm wire, as shown in Table 2. During the cold-drawing process, lubricating oil was used to minimize the friction between the wire and the drawing die. Annealing treatment was applied to cold-drawn Al-3.0 wt.% Mg alloy wires with 96% strain at different temperatures for 1 hour. The microstructure and mechanical properties of the annealed alloy wires were tested to analyze the relationship between the microstructure evolution and the mechanical property change of the alloy wires annealed at different

temperatures.

**Table 2.** The diameter of the alloy wires after each drawing pass

Pass	1	2	3	4	5	6	7	8	9	10	11	12	13	14	15
Diameter(mm)	9.0	8.0	7.0	6.0	5.0	4.5	4.0	3.8	3.5	3.2	3.0	2.8	2.5	2.2	2.0
Strain(%)	19.0	36.0	51.0	64.0	75.0	79.8	84.0	85.6	87.8	89.8	91.0	92.2	93.8	95.2	96.0

### 2.3 Recrystallization temperature measurement

During the annealing processing, the recrystallization of cold-drawn aluminium alloy happens with grain nucleation and growth. The recrystallization temperature of the deformed alloy is not a constant value, but influenced by many factors such as alloy composition, deformation extent, etc. In this paper, the softening curve method was applied to estimate the recrystallization temperature of the cold-drawn Al-3.0 wt.% Mg alloy wires with 96% strain. The cold-drawn wires were annealed at 200 °C, 250 °C, 300 °C, 325 °C, 350 °C, 375 °C, 400 °C, 425 °C, 450 °C, 475 °C and 500 °C for 1 hour. The Vickers hardness of the annealed alloy wires was tested. The recrystallization fraction of the alloy can be calculated by the hardness value, as shown in Equation (1):

$$X_i = \frac{H_{\max} - H_i}{H_{\max} - H_{\min}} \quad (1)$$

where  $X_i$  is the recrystallization fraction.  $H_i$  is the hardness value of annealed alloy wire at different temperature,  $H_{\max}$  is the maximum hardness value of the alloy wire, which is the hardness value of the cold-drawn alloy wire with 96% strain in this paper, and  $H_{\min}$  is the minimum hardness value of the alloy wire with perfect recrystallization. In this work, the recrystallization temperature of the cold-drawn Al-3.0 wt.% Mg alloy wire with 96% strain was defined as the temperature at which the recrystallization fraction was 95%.

### 2.4 Mechanical properties test

The mechanical properties of alloy wires annealed at 250 °C, 300 °C, 350 °C, 400 °C, 450 °C and 500 °C were tested. According to GB/T 228-2002, the length and gauge of the tensile specimen were both 200 mm. Tensile test was carried out at a strain rate of 2 mm/min.

### 2.5 Microstructure analysis

The cross sections of cold-drawn Al-3.0 wt.%Mg alloy wires with 96% strain and the alloy wires annealed at 250 °C, 350 °C and 450 °C were prepared as shown in Fig. 1 and tested by Hitachi S-3400N scanning electron microscopy (SEM) and Olympus-BX51M optical microscopy (OM). Both the grain size and the second phase particle size were measured by Image J software. The grain of the cold-drawn alloy was elongated, and it was difficult to measure the grain diameter. In tensile test, when the tensile direction was parallel to the drawing direction, the grain boundary spacing along the stretched drawing

direction can be considered as the grain diameter to analyze the relationship between grain size and mechanical properties in the drawing direction. Inverse pole figures and Orientation Distribution Function (ODF) maps were collected by Bruker D-8 Discover (2D detector) X-ray diffraction according to Schulz reflection method.

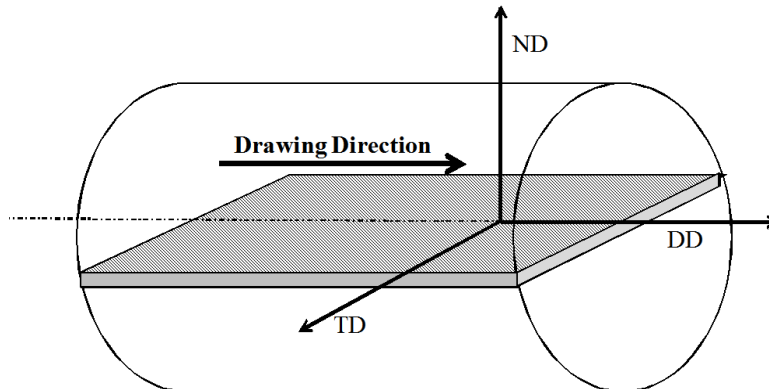


**Figure 1.** Schematic diagram of sample option for structure analysis

### 2.6 Immersion test and electrochemical measurement

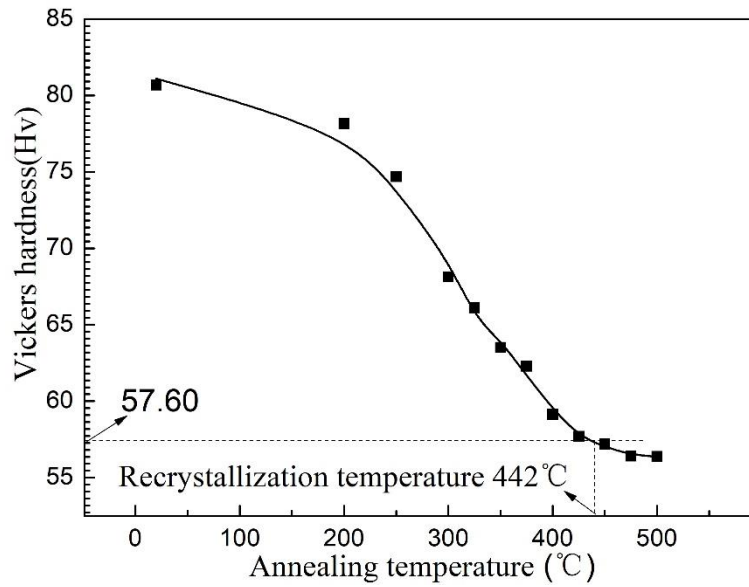
The corrosion test was performed on cold-drawn Al-3.0wt.%Mg alloy wires and Al-3.0wt.%Mg alloy wires annealed at 450 °C. In addition, the immersion test and electrochemical measurement were conducted in an unsaturated 3.5 wt.%NaCl solution, and then the specimens were kept in NaCl solution for 120 hours. The electrochemical measurement was conducted using the PARSTAT 2273 electrochemical workstation, which used a three-electrode system, including working electrode (specimen), reference electrode (232 model saturated calomel electrode) and auxiliary electrode (213 model Pt wire). After the open circuit potential was stable, electrochemical impedance spectroscopy (EIS) and potentiodynamic polarization were tested according to ASTM G3-13. In particular, EIS test was performed at a frequency of  $10^5$  to  $10^{-2}$  Hz, while the scanning rate of potentiodynamic polarization experiment was 0.1 mV/s. All the measurements were repeated at least three times to ensure the accuracy of the results.

## 3. RESULTS AND DISCUSSION

### 3.1 Microstructure

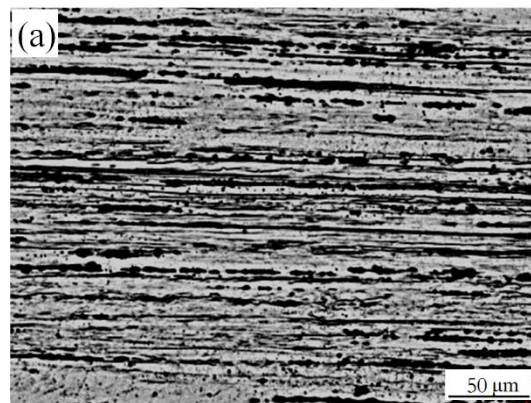
The Recrystallization softening curves of the Al-3.0 wt.% Mg alloy wire with 96% strain annealed at different temperatures are shown in Fig. 2. As the annealing temperature increased, the Vickers hardness of the annealed Al-3.0 wt.% Mg alloy gradually decreased. When the annealing temperature achieved 475 °C, the Vickers hardness reached a stable value. According to Equation (1) and the softening curve, when the recrystallization fraction was 95%, the Vickers hardness was 57.6 Hv. The results indicated that the recrystallization temperature of the cold-drawn Al-3.0 wt.% Mg alloy wire

with 96% strain was 442 °C.



**Figure 2.** Recrystallization softening curve of Al-3.0 wt.%Mg alloy wire

Fig. 3 shows the microstructure and grain size distribution of Al-3.0 wt.% alloy wires with 96% strain annealed at different temperatures. In the cold-drawn alloy wire, the grain and dendrite boundaries were arranged in a lamellar structure along the drawing direction. After 1-hour annealing treatment at 250 °C, some small size recrystallized grains appeared. As the annealing temperature increased, the size of the recrystallized grains increased.



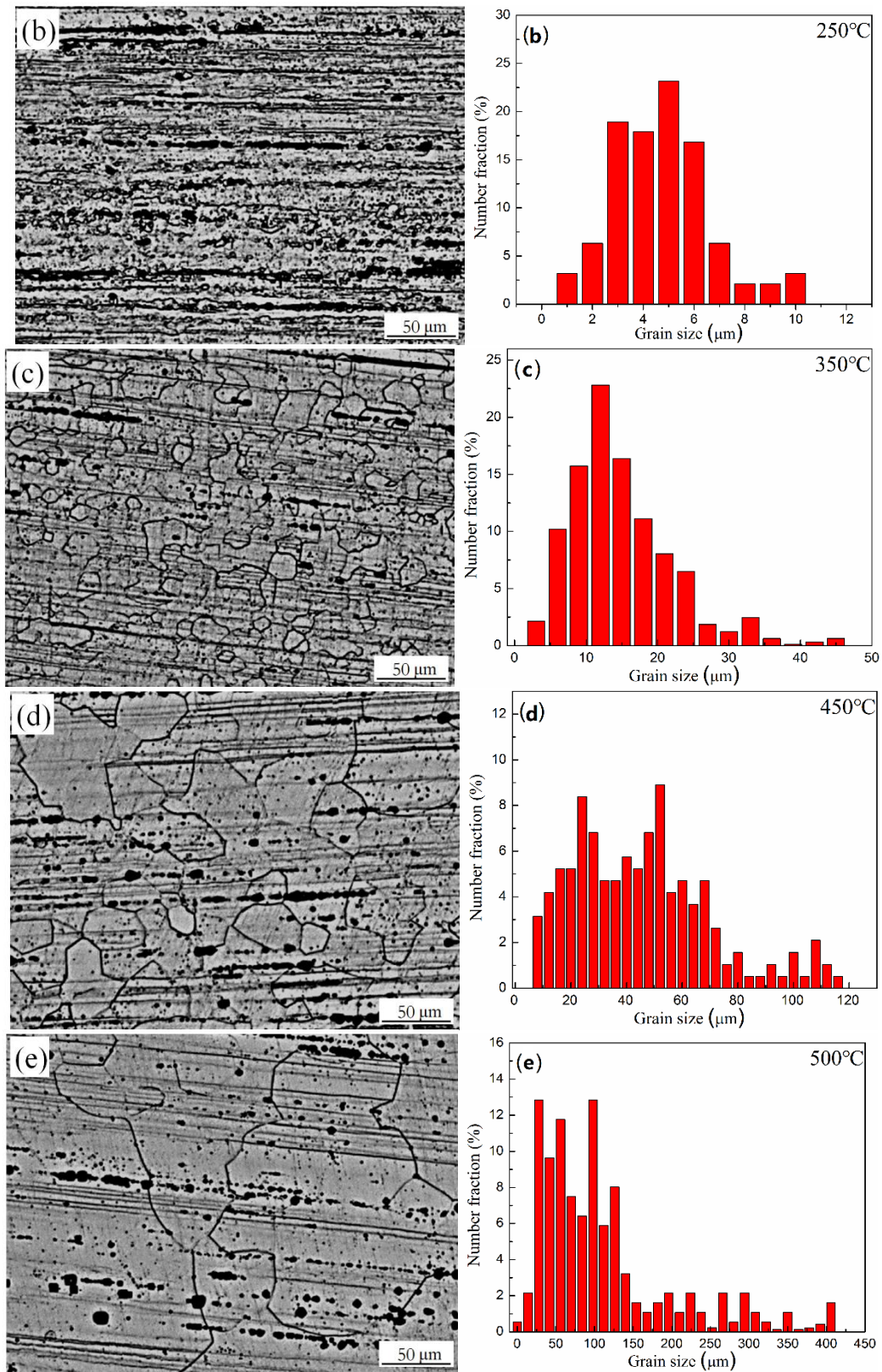
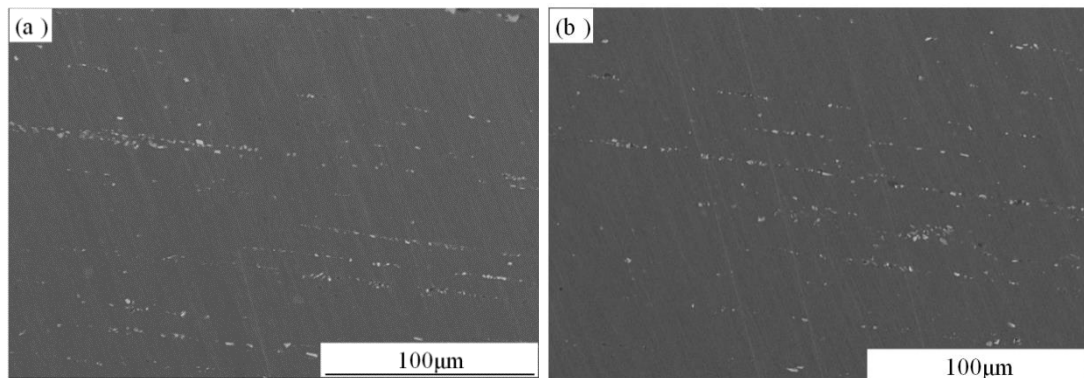


**Figure 3.** Microstructure and grain size distribution of Al-3.0 wt.% alloy wire with 96% strain annealed at different temperatures: (a) cold-drawn alloy wire; (b) alloy wire annealed at 250 °C; (c) alloy wire annealed at 350 °C, (d) alloy wire annealed at 450 °C, and (e) alloy wire annealed at 500 °C.

The grain size distribution of the alloy wires annealed at 250, 350 and 450 °C was relatively

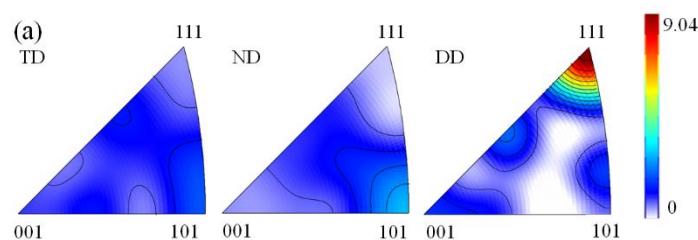
homogeneous. However, abnormal grain growth was observed in the alloy wire annealed at 550 °C, and the grain distribution became non-uniform.

During the cold-drawing process, the second phase particles in Al-3.0 wt.% Mg alloy were fragmented from skeletal shape to finer globular form, and were arranged in lines along the drawing direction, as shown in Fig. 4 (a). The second phase particles of the alloy wire annealed at 450 °C are shown in Fig. 4 (b). From the figure, they had the same form and size as the cold-drawn alloy wire, which indicated that there was no reaction on the second phase particles during the annealing process.



**Figure 4.** SEM images of cold-drawn and annealed Al-3.0wt.% Mg alloy wire: (a) cold-drawn alloy wire; (b) alloy wire annealed at 450 °C.

Fig. 5 shows the inverse pole diagrams of Al-3.0 wt.% alloy wires with 96% strain annealed at different temperatures. The cold-drawn Al-3.0 wt.% Mg alloy with 96% strain exhibited an ideal  $\langle 111 \rangle$  fiber texture with a high intensity of 9.04. When the alloy wires were annealed at 250, 350 and 450 °C for 1 hour, the intensity of  $\langle 111 \rangle$  fiber texture decreased to 8.34, 5.44 and 4.60, respectively. Meanwhile,  $\langle 001 \rangle$  texture appeared in the alloy wire annealed at 450 °C. During the annealing process, some recrystallized grains transformed from  $\langle 111 \rangle$  orientation to other orientations, and the proportion of the grains in  $\langle 111 \rangle$  orientation decreased. When the annealing temperature was higher, more recrystallized grains were generated. In addition, there were more grains in  $\langle 001 \rangle$  orientation than in other orientations. As a result, with the increase of the annealing temperature, the intensity of  $\langle 111 \rangle$  texture in the annealed alloy decreased, while the intensity of  $\langle 001 \rangle$  texture increased.



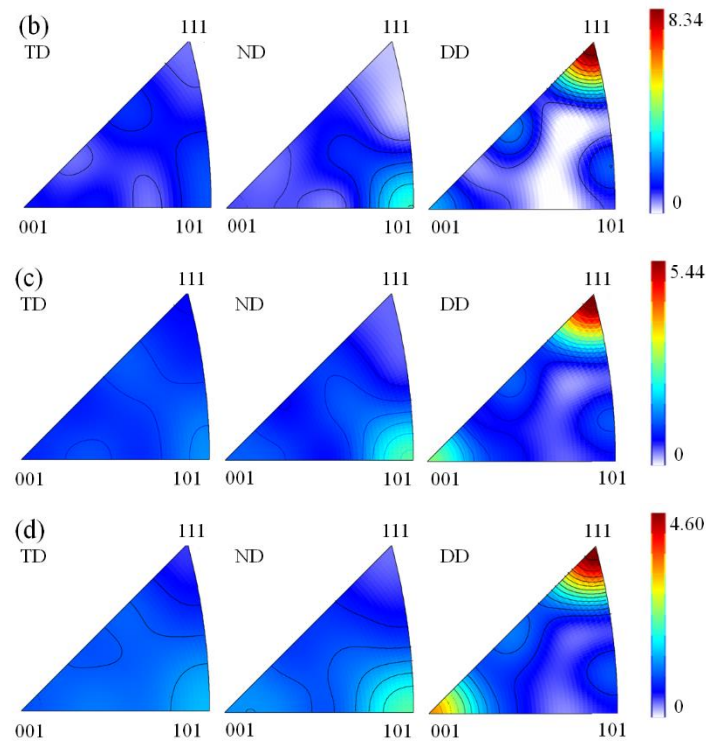


**Figure 5.** The inverse pole diagrams of Al-3.0 wt.% Mg alloy wire with 96% strain annealed at different temperatures: (a) cold-drawn alloy wire; (b) alloy wire annealed at 250 °C; (c) alloy wire annealed at 350 °C; (d) alloy wire annealed at 450 °C.

Fig. 6 shows the ODFs map of Al-3.0 wt.% Mg alloy wire with 96% strain annealed at different temperatures. The orientation intensity of texture component was calculated by Jtex software, as shown in Fig. 7. In the cold-drawn Al-3.0 wt.% Mg alloy with 96% strain, the texture components with high intensity, i.e., Copper  $\{112\}\langle 111\rangle$ , Brass  $\{001\}\langle 211\rangle$  and S  $\{123\}\langle 634\rangle$  existed. After 1-hour annealing treatment at 250, 350 and 450 °C, the intensity of Copper  $\{112\}\langle 111\rangle$  texture decreased from 9.54 to 8.85, 5.75 and 4.92, respectively, the intensity of Brass  $\{001\}\langle 211\rangle$  texture decreased from 2.19 to 2.09, 1.96 and 1.42, respectively, and the intensity of S  $\{123\}\langle 634\rangle$  texture decreased from 2.10 to 1.51, 1.46 and 1.50, respectively. With the increase of annealing temperature, the intensity of Copper  $\{112\}\langle 111\rangle$  and Brass  $\{001\}\langle 211\rangle$  texture decreased continually. However, the annealing temperature had no obviously influence on the intensity of S  $\{123\}\langle 634\rangle$  texture. The higher the annealing temperature, the more recrystallized grains were generated, and the less remaining grains in Copper  $\{112\}\langle 111\rangle$ , Brass  $\{001\}\langle 211\rangle$  and S  $\{123\}\langle 634\rangle$  orientation. During the annealing process, as the annealing temperature increased, the intensity of Cube  $\{001\}\langle 100\rangle$  and Cube-DD  $\{013\}\langle 100\rangle$  increased. The result indicated that more recrystallized grains in Cube  $\{001\}\langle 100\rangle$  and Cube-DD  $\{013\}\langle 100\rangle$  orientation were generated than in other orientations.

During the annealing process of the deformed metal, the recrystallization texture form in some specific orientation can be influenced by many factors, including the deformation extent, alloy composition, the shape and size of the second phase, the initial texture, etc. [13-16]. Recrystallization nucleation is complicated and the mechanism is difficult to explain. Theories of directional nucleation and directional growth are complementary to explain the recrystallization nucleation mechanism. During the annealing process, subgrains in Cube  $\{001\}\langle 100\rangle$  and Cube-DD  $\{013\}\langle 100\rangle$  orientations can

recover quickly and have a high nucleation potential [17]. As a result, recrystallized grains prefer to grow in these two orientations. In FCC metals, grain boundaries in  $40^\circ \langle 111 \rangle$  orientation have the highest migration velocity. Therefore, the grains in this orientation grow very fast. At the same time, grains in  $40^\circ \langle 111 \rangle$  orientation usually grow into the nearby grains in Cube orientation. Therefore, recrystallized grains in Cube  $\{001\} \langle 100 \rangle$  and Cube-DD  $\{013\} \langle 100 \rangle$  orientations have a high growth rate. Since the grains in Cube  $\{001\} \langle 100 \rangle$  and Cube-DD  $\{013\} \langle 100 \rangle$  orientations have advantages for both nucleation and growth, Cube and Cube-DD texture will be formed first in the annealing process. When the annealing temperature was higher, more recrystallized grains were generated, and the recrystallized grains were bigger. And more grains generated in  $\langle 100 \rangle$  orientation caused the intensity of  $\langle 100 \rangle$  texture to increase, as shown in Fig. 5. As a result, as the annealing temperature increased, the intensity of Cube  $\{001\} \langle 100 \rangle$  and Cube-DD  $\{013\} \langle 100 \rangle$  texture increased.

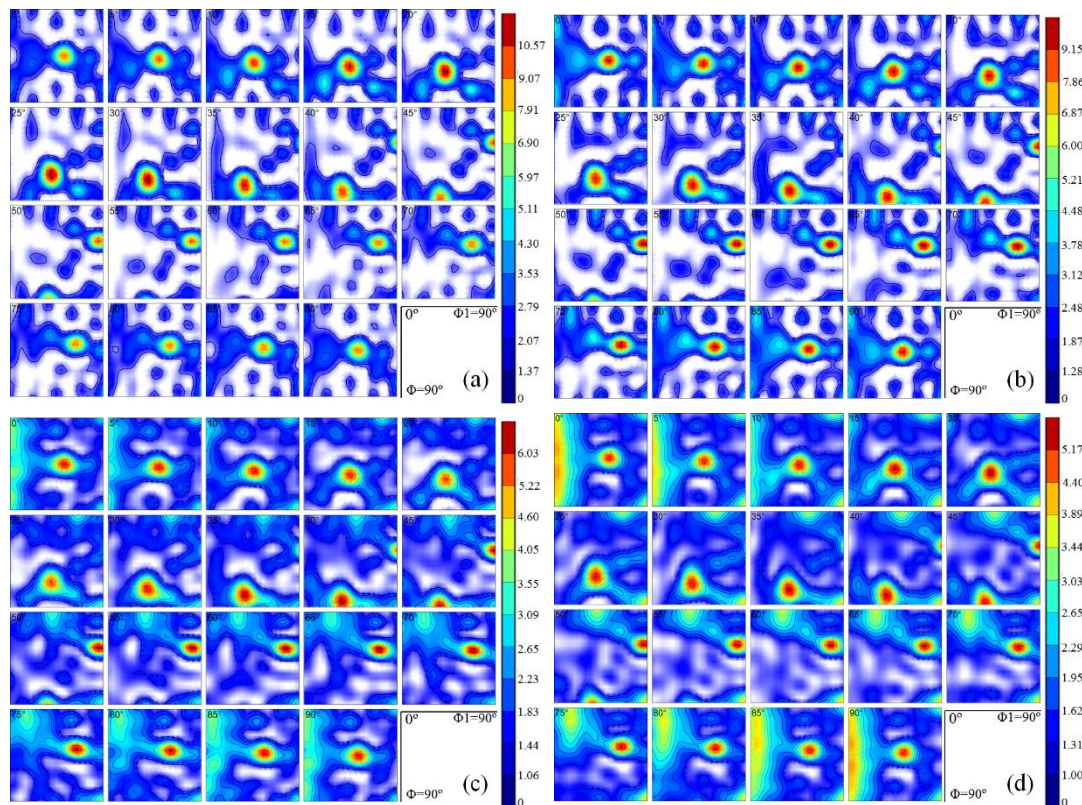


**Figure 6.** The ODF maps of Al-3.0 wt.% Mg alloy wire with 96% strain annealed at different temperatures: (a) cold-drawn alloy wire; (b) alloy wire annealed at 250 °C; (c) alloy wire annealed at 350 °C; and (d) alloy wire annealed at 450 °C.

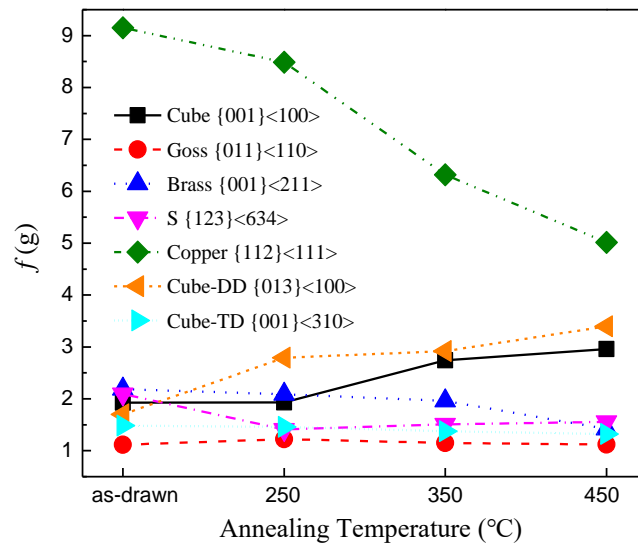


**Figure 7.** Relationship between the orientation intensity of texture component and annealing temperature

### 3.2 Mechanical Properties

Fig. 8 shows the tensile strength, yield strength, and elongation to failure curves of Al-3.0 wt.% Mg alloy wire with 96% strain annealed at different temperatures. As the annealing temperature increased, the tensile strength of the alloy wire decreased linearly, while the yield strength exhibited a three-stage characteristic decrease. Specifically, the tensile strength of the alloy wire had a significant reduction when the annealing temperature was in the range of 250 to 300 °C, which was caused by the appearance of recrystallized grains at the annealing temperature of above 250 °C. As the annealing temperature increased above 450 °C, the elongation to failure first increased and then decreased.

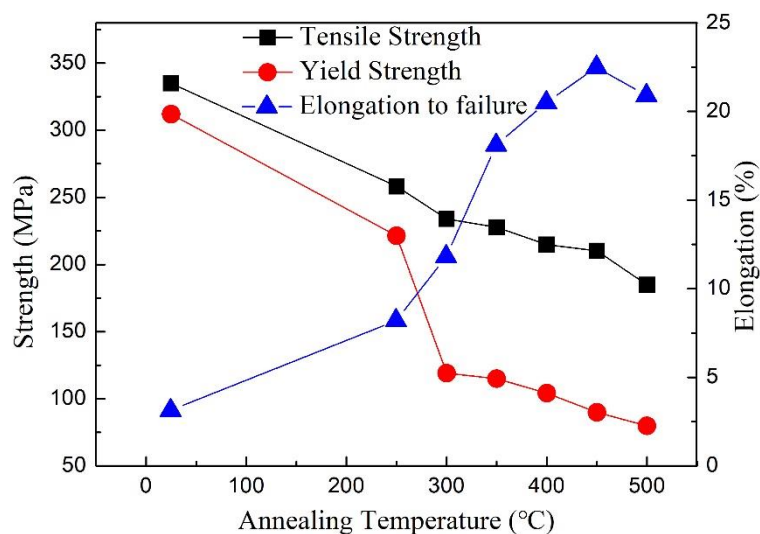


**Figure 8.** Tensile strength, yield strength and elongation to failure of Al-3.0 wt.% Mg alloy wire with 96% strain annealed at different temperatures.

**Table 3.** Microstructure and mechanical properties of Al-3.0 wt.%Mg alloy wire with 96% strain annealed at different temperatures (°C)

Annealing temperature (°C)	cold-drawn	250	350	450
Intensity of texture (level)	10.57	9.15	6.03	5.17
Grain size (μm)	5.03	8.96	42.12	68.23
Ultimate tensile strength (MPa)	334.60	258.21	227.66	210.14
Yield strength (MPa)	312.01	221.39	114.95	89.91
Elongation to failure (%)	3.13	8.20	18.12	22.53

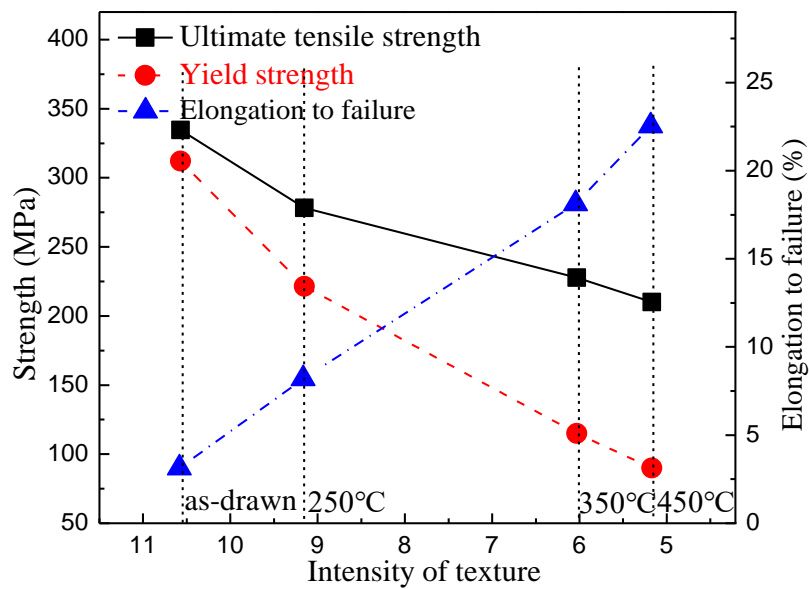
During the annealing process, due to the comprehensive effect of microstructure evolution, including evolutions of texture, grain size, second phase, dislocation dissociation, stress release, et al., the strength of Al-3.0 wt.% Mg alloy wire with 96% strain increased and the plasticity decreased. The shape and size of second phase particles in the alloy wires did not have obvious changes in the annealing process, as shown in Fig. 4. In order to analyze the relationship between microstructure evolution and the change in mechanical properties, the intensity of texture, grain size, strength and elongation to failure of Al-3.0 wt.% Mg alloy wire with 96% strain annealed at 250, 350 and 450 °C were tested, and the results are listed in Table 3. Dislocation dissociation and stress release have a significant effect on the mechanical properties. However, it is difficult to quantify the dislocation dissociation and stress release. Therefore, the effects of the dislocation and stress on mechanical properties were analyzed qualitatively.

Fig. 9 shows the relationship between the mechanical properties and texture intensity of the annealed Al-3.0 wt.% Mg alloy wire. High intensity Copper {112}<111> texture and <111> fiber texture existed in the cold-drawn alloy wire with 96% strain. The strength of the metals is mainly determined by the critical resolved shear stress and the Schmid factor [18,19]. Since the critical resolved shear stress is usually fixed, the strength should be inversely proportional to the Schmid factor. The grains in the orientation with a low Schmid factor are hard to slip due to their higher resolved shear stress. As a result, the grains with a low Schmid factor have low plasticity. Copper texture and <111> fiber texture have the lowest Schmid factor (0.272) and are considered as the hard orientation during the plastic deformation [20]. Thus, the presence of Copper and <111> fiber texture will lead to a high strength and low plasticity of the alloys [21,22]. During the annealing process, the intensity of Copper texture, <111> fiber texture and the amount of grains in these hard orientations decreased, leading to decreased strength and increased plasticity. At the same time, recrystallization Cube and Cube-DD texture were formed. However, the intensity of recrystallization texture with the Schmid factor of 0.408 formed during the annealing process was so low that it had no obvious influence on the variation of strength and plasticity. When the annealing temperature was higher, the intensity of the deformation texture was further decreased, the strength was further reduced, and the plasticity was further increased. The relationship between texture intensity and tensile strength ( $R_m$ ) / yield strength ( $R_{p0.2}$ ) / elongation to failure ( $A$ ) was linear and can be expressed by Equations (2), (3) and (4).

$$R_m = 21.5277I_t + 96.2432, r^2 = 0.9439 \quad (2)$$

$$R_{p0.2} = 39.6862I_t - 122.2096, r^2 = 0.9689 \quad (3)$$

$$A = -3.479I_t + 39.8940, r^2 = 0.9934 \quad (4)$$



**Figure 9.** Relationship between the mechanical properties and texture intensity of the annealed Al-3.0 wt.%Mg alloy wire.

The relationship between the mechanical properties and grain size of annealed Al-3.0 wt.% Mg alloy wires is shown in Fig. 10. As shown in Hall-Petch relation, the yield strength of alloys is linearly dependent on the grain size  $d_g^{-1/2}$ . Thus, the relationship between mechanical property and  $d_g^{-1/2}$  is shown in Fig. 10(b). As the recrystallized grain size increased, the strength of the alloy decreased. The relationship between  $d_g^{-1/2}$  and tensile strength/yield strength was linear and can be expressed by Equations (5) and (6).

$$R_m = 362.0860d_g^{-1/2} + 167.1420, \quad r^2 = 0.9749 \quad (5)$$

$$R_{p0.2} = 665.8110d_g^{-1/2} + 8.9403, \quad r^2 = 0.9928 \quad (6)$$

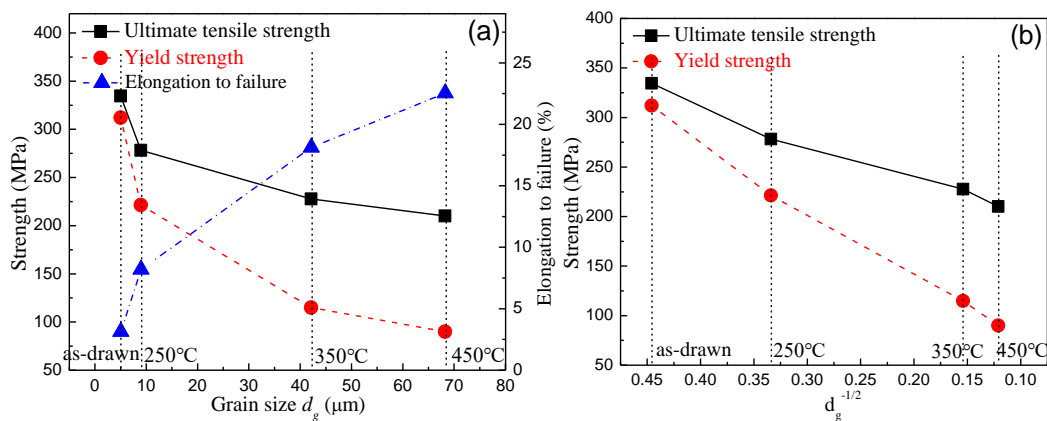


**Figure 10.** Relationship between the mechanical properties and grain size of annealed Al-3.0 wt.%Mg alloy wires.

When the annealing temperature was higher, the generated recrystallized grains were bigger, and the strength of the alloy was lower. Theoretically, large grain size was not beneficial to the plasticity of the alloy. However, as the recrystallized grain increased, the plasticity of the alloy increased, which was contrary to the theory. During the annealing process, the improving of the plasticity benefited from not only the dislocation dissociation and stress release at a high temperature but also the decrease in the texture intensity as stated before. The relationship between the texture intensity, grain size and strength of the annealed alloys was calculated and expressed by Equations (7) and (8).

$$R_m = 232.071 - 19.3397I_t + 682.6929d_g^{-1/2}, \quad r^2 = 0.9892 \quad (7)$$

$$R_{p0.2} = 83.9023 - 22.3280I_t + 1035.9520d_g^{-1/2}, \quad r^2 = 0.9976 \quad (8)$$

### 3.3 Corrosion behavior

Fig.11 shows the surface morphologies of Al-3.0 wt.% Mg alloys before and after annealing treatment at 450 °C immersed in 3.5 wt.% NaCl solution for 120 hours. After the annealing treatment, pitting holes appeared around the second phases of the immersed alloys. There was no significant difference in the amounts of pitting holes on cold-drawn alloys and annealed alloys. However, the size of pitting holes on the surface of cold-drawn alloy was much bigger than that of annealed alloy. The result indicated that the pitting sensibility between cold-drawn alloy and annealed alloy was similar, but the annealed alloy had better corrosion resistance. As a result, the pitting growth rate of annealed alloy was slower than that of cold-drawn alloy.

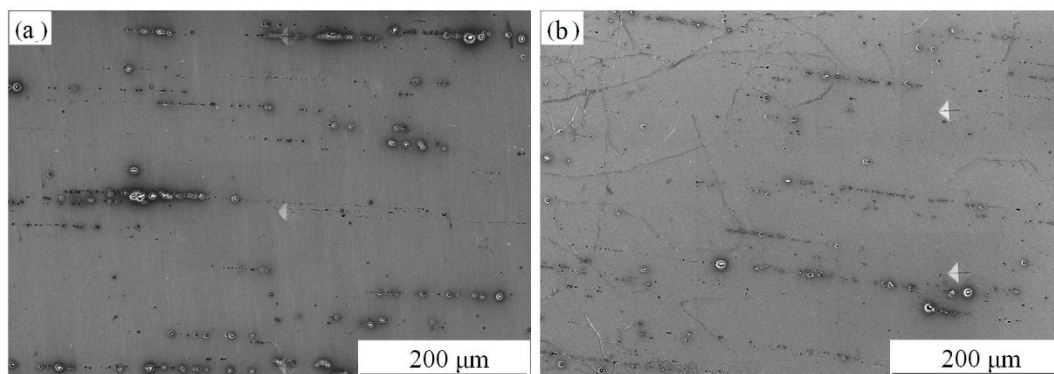


**Figure 11.** Surface morphologies of Al-3.0wt.%Mg alloys before and after annealing treatment at 450 °C immersed in 3.5 wt.% NaCl solution for 120 hours (a) Al-3.0 wt.%Mg alloy before annealing treatment; (b) Al-3.0 wt.%Mg alloy after annealing treatment

Fig.11 shows the potentiodynamic polarization curves of Al-3.0Mg alloys before and after annealing treatment at 450 °C. The corrosion potential ( $E_{corr}$ ), corrosion current density ( $i_{corr}$ ), and pitting corrosion potential ( $E_{pit}$ ) are summarized in Table 4. There were no significant differences in the corrosion and pitting potential between cold-drawn and annealed alloys. However, the annealed alloy had a much lower corrosion current density than the cold-drawn alloy. The result indicated that annealing

treatment at 450 °C had no obvious effect on corrosion and pitting sensibility of cold-drawn Al-3.0 wt.% Mg alloy, but it can significantly reduce the corrosion rate.

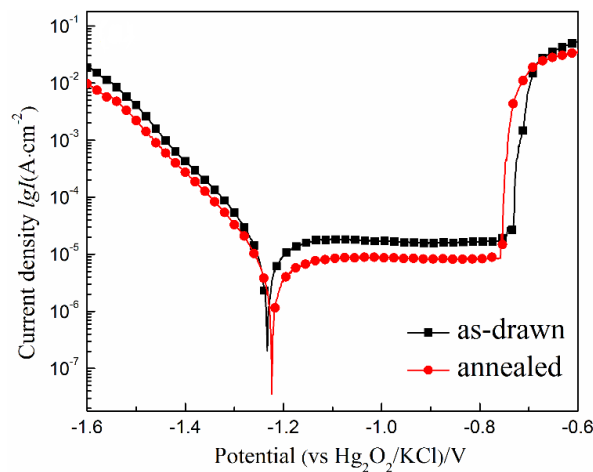


**Figure 12.** Potentiodynamic polarization curves of Al-3.0 wt.%Mg alloys before and after annealing treatment at 450 °C

**Table 4.**  $E_{corr}$ ,  $i_{corr}$ ,  $E_{pit}$  values of Al-3.0 wt.%Mg alloys before and after annealing treatment at 450°C

	$E_{corr}/V$	$i_{corr}/\mu A \cdot cm^{-2}$	$E_{pit}/V$
Cold-drawn	-1.223	6.659	-0.766
Annealed	-1.220	4.234	-0.763

The Nyquist diagram of Al-3.0 wt.% Mg alloys before and after annealing treatment at 450 °C is shown in Fig. 13. The EIS of the tested alloys can be represented by the equivalent circuit in Fig. 14.  $R_t$  represents the activity of the alloys and  $R_{t(pit)}$  represents the resistance of ion diffusion through the passive films. The higher the values of  $R_t$  and  $R_{t(pit)}$ , the lower the activity of the alloys, and the more stable and denser the passive films. In this study, the parameters of the equivalent circuit were calculated by ZSimpWin software, and the results are summarized in Table 5. In general, the diameter of the capacitive circle is associated with the charge transfer resistance. The larger the diameter of the capacitor circle, the slower the corrosion rate, and the better the corrosion resistance. Compared to cold-drawn alloys, annealed alloys had a larger capacitor circle diameter, a higher value of  $R_t$ , and a larger value of  $R_{t(pit)}$ . The result indicated that annealing treatment at 450 °C could increase the corrosion resistance and decrease the corrosion rate of cold-drawn Al-3.0 wt.% Mg alloy.

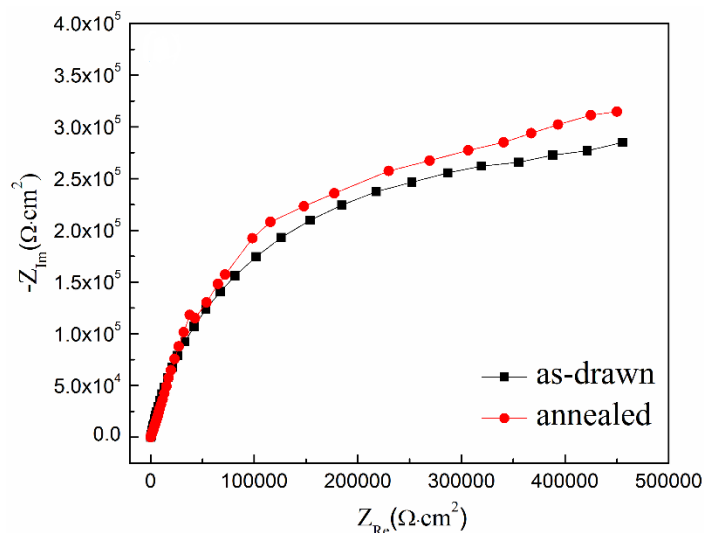


**Figure 13.** Nyquist diagram of Al-3.0 wt.%Mg alloys before and after annealing treatment at 450 °C

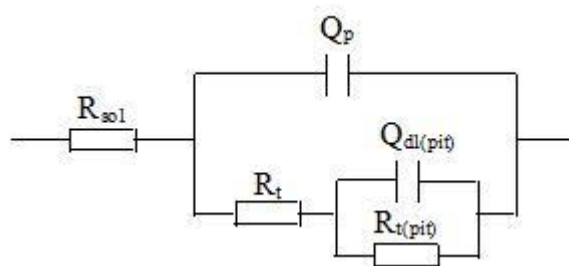


**Figure 14.** An equivalent circuit for the tested alloys

**Table 5.** The parameters of the equivalent elements in equivalent circuit for different alloys.

	$R_{sol}$ ( $\Omega \cdot \text{cm}^2$ )	$Q_p$ ( $\Omega^{-1} \cdot \text{cm}^{-2} \cdot \text{s}^{-1}$ )	n1	$R_t$ ( $\Omega \cdot \text{cm}^2$ )	$Q_{dl}$ ( $\Omega^{-1} \cdot \text{cm}^{-2} \cdot \text{s}^{-1}$ )	n2	$R_{t(pit)}$ ( $\Omega \cdot \text{cm}^2$ )
Cold-drawn	23.67	$2.76 \times 10^{-6}$	0.8448	$12.87 \times 10^4$	$3.34 \times 10^{-6}$	0.9289	$22.14 \times 10^4$
Annealed	18.28	$2.31 \times 10^{-6}$	0.9877	$19.39 \times 10^4$	$4.51 \times 10^{-6}$	0.9267	$30.32 \times 10^4$

Annealed alloys had better corrosion resistance than cold-drawn alloys. However, annealed alloys and cold-drawn alloys had similar pitting corrosion sensibility. During the annealing process, no obvious reaction was observed on the second phase particles. As mentioned above, the pitting corrosion generally occurred at the position of the second phases [12, 23-24]. The pitting corrosion sensibility of Al-Mg alloys were related to the amount and the size of the second phases. The more and bigger the second phases, the more and larger the pitting holes would be. As a result, annealing treatment had no obvious effect on pitting corrosion sensibility of cold-drawn Al-3.0 wt.% Mg alloy. However, dislocation dissociation, stress release, and formation of recrystallized grain at high temperature were all beneficial to the improvement in the corrosion resistance of cold-processed alloys. As a result, after 450 °C annealing treatment, the corrosion rate of Al-3.0 wt.% Mg alloy decreased.

#### 4. CONCLUSIONS

The influence of annealing temperature on the microstructure and mechanical properties of Al-3.0 wt% Mg alloy wire with 96% strain was investigated. The following conclusions can be obtained from the results:

(1) The recrystallization temperature of cold-drawn Al-3.0 wt.% Mg alloy with 96% strain obtained by softening curve method was 442 °C. During the annealing process, recrystallized grain appeared, while no changes were observed on the second phase particles. As the annealing temperature increased, the size of the recrystallized grains increased. Abnormal grain growth was observed in the alloy wire annealed at 550 °C

(2) During the annealing process, the intensity of deformation texture decreased, while Cube {001}<100> and Cube-DD {013}<100> recrystallization texture appeared. The higher the annealing temperature, the fewer remaining grains in Copper {112}<111>, Brass {001}<211> and S {123}<634> orientations, and the more recrystallized grains in Cube {001}<100> and Cube-DD {013}<100> orientations.

(3) As the annealing temperature increased to above 450 °C, the tensile strength of the alloy wires decreased linearly, while the yield strength exhibited a three-stage characteristic decrease, and the elongation to failure first increased and then decreased.

(4) The relationship between the texture intensity, grain size and strength of the alloy was linear and can be expressed by the equations of  $R_m=232.071-19.3397I_t+682.6929d_g^{1/2}$  and  $R_{p0.2}=83.9023-22.3290 I_t+1035.9520 d_g^{1/2}$ .

(5) Annealing treatment had no obvious effect on pitting corrosion sensibility of cold-drawn Al-3.0 wt.% Mg alloy. However, after 450 °C annealing treatment, the corrosion rate of the alloys decreased due to dislocation dissociation, stress release and formation of recrystallized grains at high temperature.

#### ACKNOWLEDGEMENTS

This study was financially supported by “National Science Foundation of China (51909071), Natural Science Foundation of Jiangsu Province (BK20190493) and the Fundamental Research Funds for the Central Universities (B200202133).

#### References

1. Z.G. Wu, M. Song and Y.H. He, *Mater. Sci. Eng. A.*, 504 (2009) 183.
2. H.H. Chen, J.Y. Wang, J. Lee and S. Lee, *J. Alloy. Compd.*, 460 (2008) 305.
3. M.M. Sharma and C.W. Ziemian, *J. Mater. Eng. Perform.*, 17 (2008) 870.
4. W.C. Xiao, B.Y. Wang, Y. Kang, W.P. Ma and X.F. Tang, *Rare Metals*, 36 (2017) 485.
5. K.R. Narayanan and S.S. Subbiah, *Appl. Phys. A-Mater.*, 107 (2012) 485.
6. T.S. Cao, C. Vachey, P. Montmitinnet and P.O. Bouchard, *J. Mater. Process. Tech.*, 217 (2015) 30.
7. C.S. Cetinarslan, *Indian J. Eng. Mater. S.*, 19 (2012) 221.
8. P. Kustra, A. Milenin, D. Byrska-Wójcik, O. Grydin and M. Schaper, *J. Mater. Process. Tech.*, 247 (2017) 234.
9. H.S. Yu, W.P. Yang, H.B. Cui, X.F. Guo, Y. Wang and Y.L. Wu, *J. Wuhan Univ. Technol.*, 34 (2019) 154.
10. W.W. Lei, D. Zhu, H.X. Wang and W. Liang, *J. Wuhan Univ. Technol.*, 34 (2019) 1193.

11. X. Zhang, Z.H. Wang, Z.H. Zhou and J. Shao, *Appl. Phys. A-Mater.*, 124 (2018) 690.
12. X. Zhang, Z.H. Wang, Z.H. Zhou, J. Cao and G.H. Yang, *Inter. J. of Electrochem. Sci.*, 15 (2020) 1727.
13. O. Engler, *Metall. Mater. Trans. A.*, 30A (1999) 1517.
14. W.C. Liu, T. Zhai and J.G. Morris, *Mater. Sci. Eng. A.*, 358 (2003) 84.
15. K. Lücke and O. Engler, *Mater. Sci. Tech.*, 6 (1990) 1113.
16. K. Sjolstad, *Mater. Sci. Foru.*, 408-412 (2002) 1471.
17. R.D. Doherty, K. Kashyap and S. Panchanadeswaran, *Acta Mater.*, 41 (1993), 3029.
18. T.A. Parthasarathy, S.I. Rao, D.M. Dimiduk, M.D. Uchic and D.R. Trinkle, *Scripta Mater.*, 56 (2007) 313.
19. J.P. Hou, Q. Wang and H.J. Yang, *Mater. Sci. Eng. A.*, 639 (2015) 103.
20. I.J. Beyerleina and L.S. Tóth, *Prog. Matet. Sci.*, 54 (2009) 427.
21. Q. Zeng, X. Wen and T. Zhai, *Metall. and Mat. Trans. A.*, 40 (2009) 2488.
22. Q. Liu, Z.Y. Yao, A. Godfrey and W. Liu, *J. Alloy. Compd.*, 482 2009 264.
23. X. Zhang, Z.H. Wang, Z.H. Zhou and J.M. Xu, *J. Alloys Compd.*, 698 (2017) 241.
24. X. Zhang, Z.H. Wang, Z.H. Zhou and Jianming Xu, *J. Mater. Eng. Perform.*, 25 (2016) 1122.

© 2021 The Authors. Published by ESG ([www.electrochemsci.org](http://www.electrochemsci.org)). This article is an open access article distributed under the terms and conditions of the Creative Commons Attribution license (<http://creativecommons.org/licenses/by/4.0/>).